A thumbnail-based hierarchical fuzzy clustering algorithm for SAR image segmentation

Shang, Ronghua; Chen, Chen; Wang, Guangguang; Jiao, Licheng; Okoth, Michael Aggrey; Stolkin, Rustam

DOI:
10.1016/j.sigpro.2020.107518

Document Version
Peer reviewed version

Citation for published version (Harvard):
Shang, R, Chen, C, Wang, G, Jiao, L, Okoth, MA & Stolkin, R 2020, 'A thumbnail-based hierarchical fuzzy clustering algorithm for SAR image segmentation', *Signal Processing*, vol. 171, 107518, pp. 1-15. https://doi.org/10.1016/j.sigpro.2020.107518

A thumbnail-based hierarchical fuzzy clustering algorithm for SAR image segmentation

Ronghua Shang , Chen Chen , Guangguang Wang ,
Licheng Jiao , Michael Aggrey Okoth , Rustam Stolkin

PII: S0165-1684(20)30061-X
DOI: https://doi.org/10.1016/j.sigpro.2020.107518
Reference: SIGPRO 107518

To appear in: *Signal Processing*

Received date: 5 May 2019
Revised date: 11 January 2020
Accepted date: 1 February 2020

Please cite this article as: Ronghua Shang , Chen Chen , Guangguang Wang , Licheng Jiao , Michael Aggrey Okoth , Rustam Stolkin , A thumbnail-based hierarchical fuzzy clustering algorithm for SAR image segmentation, *Signal Processing* (2020), doi: https://doi.org/10.1016/j.sigpro.2020.107518

Highlights

- This paper proposes a novel algorithm for segmentation of SAR image.
- THFCM firstly divides the image into pixel groups to extract local feature.
- The major pixels of each pixel group are selected to construct a thumbnail.
- The thumbnail approach leverages local image information, helping to overcome speckle noise.
- Experiments suggest that THFCM outperforms several other state-of-the-art algorithms in terms of both segmentation accuracy and running time.

A thumbnail-based hierarchical fuzzy clustering algorithm for SAR image segmentation

Ronghua Shang[a], Chen Chen[a], Guangguang Wang[a], Licheng Jiao[a], Michael Aggrey Okoth[a], and Rustam Stolkin[b]
(a. Key Laboratory of Intelligent Perception and Image Understanding of Ministry of Education, International Research Center for Intelligent Perception and Computation, School of Artificial Intelligence, Xidian University, Xi'an, Shanxi Province 710071, China. b. the Extreme Robotics Lab, University of Birmingham, UK.)

***Abstract*—**This paper proposes a novel algorithm for segmentation of synthetic aperture radar (SAR) image, our proposed algorithm (THFCM) is based on thumbnail image representations and a hierarchical fuzzy C-means (FCM) approach. THFCM firstly divides the image into pixel groups to extract local feature, and the major pixels of each pixel group are selected to construct a thumbnail. FCM is then used to segment each thumbnail, and hierarchical segmentation is then performed on the overall image data, based on the results of thumbnail clustering. The thumbnail approach leverages local image information, helping to overcome speckle noise, while the hierarchical approach improves computational efficiency. Experiments on simulated and real SAR images suggest that THFCM outperforms several other state-of-the-art algorithms in terms of both segmentation accuracy and running time.

***Index Terms*—**Fuzzy C-means, Neighborhood information, Speckle phenomenon, SAR image segmentation, Thumbnail.

I. INTRODUCTION

Radar-based machine vision is a rapidly evolving branch of machine intelligence. It has been extensively used in target detection, change detection and tracking, in diverse applications such as military surveillance, environmental monitoring and others [1-3]. In particular, the problem of SAR image segmentation has drawn increasing attention from many researchers [4]. However, the trade-off between suppressing speckle noise (prevalent in SAR images), while also limiting computational complexity, remains a difficult open problem. This paper attempts to tackle this problem, presenting a method based on thumbnails. These are constructed by dividing the original SAR image into a number of non-overlapping but connected homogeneous regions [5, 6].

The speckle phenomenon of SAR images is one of their inherent characteristics, which brings some difficulties to the segmentation task [7, 8]. Therefore, many conventional image segmentation methods do not yield good results on SAR images [9]. Hence, many researchers have proposed despeckling filters to improve SAR image segmentation accuracy [14]. Some methods have a filter operation before segmenting [13]. [10] extracted texture features to reduce the influence of speckle noise. Clustering results, based on the learned texture features, can improve the performance significantly [11]. The concept of non-local filtering appears to have been gradually demonstrating superior performance in recent years [15]. The method in [12] extracts features from several sub-images obtained by a Gabor filter bank, which can reduce the adverse effects of speckle noise.

There are many other algorithms trying to solve this problem of image segmentation. For example, variety of early work was based on thresholding of pixel values [16]. Expectation-Maximisation (EM) [17], and other methods, e.g. Kittler Illingworth (KI) [18], have been proposed for determining optimal threshold values. In 1988, Kass *et al.* proposed an active contour model, introducing a new approach to solve image segmentation by minimizing an energy function [19, 20]. A statistical active contour model was applied to the problem of oil slick segmentation in [21]. The level set model is one of the active contour methods [22]. The multi-layer level set method efficiently segments SAR images and promotes further image interpretation in the imaged areas [23]. Methods based on the random field model can preserve the context information in an image [24], and the Markov Random Field (MRF) as one of the typical random field models have been widely adopted [25]. Later, the conditional random field model was proposed to overcome the Markovian restriction of conditional independence [26]. The clustering methods contain many kinds of algorithms, such as spectral clustering [27], K-means clustering, FCM and others [28]. This paper makes use of the FCM algorithm and combines the idea of superpixel and despeckling filters [29].

In FCM algorithm, similar pixels are clustered into the same class by optimizing the objective function and updating membership degree for every pixel to every cluster iteratively [30]. FCM has been widely studied and applied in many fields of SAR image processing, such as change detection [31] and segmentation [32]. Many researchers have made improvements from different perspectives. A variety of improvements can be made by modifying the objective function [33], e.g. to combine cost terms from several models [34]. An adaptive fuzzy local information c-means (ADFLICM) clustering approach was proposed in [35] incorporating local spatial information. Gong *et al.* proposed a fuzzy clustering algorithm to segment the difference image in a change detection task, in which the MRF model was used to calculate the membership degree [36]. The calculation of cluster centers in FCM affects the updating operation and

consequently influences the convergence properties of algorithm. Later work by Zhang *et al.* in [37] presented a new method to calculate the clustering centers which improved the segmentation accuracy. Ju *et al.* changed proposed an alternative distance metric, of each element from its corresponding cluster center, which resulted in assigning more appropriate class labels to each pixel at each iteration [38].

Several recent FCM-based methods have demonstrated good performance in SAR image segmentation. Shang *et al.* presented an algorithm called clone kernel spatial FCM (CKSFCM), to overcome the problem of FCM's sensitivity to random initialisation conditions [39]. The immune clone algorithm is used to generate the initial cluster centers, and helps prevent the algorithm from converging on local optima. However, this method spends a large amount of computation time on initialing and clustering. In [40] Ji *et al.* proposed a non-local fuzzy clustering algorithm with between-cluster separation measure (NSFCM), which incorporates non-local spatial information using an improved non-local mean method. NSFCM makes full use of the information in the image, however this leads to information redundancy, which can be reduced by using other approaches to improve efficiency. Thus, Liu *et al.* incorporated adaptive local information into fuzzy clustering (ALFCM) [41]. This paper pays closer attention to the selection of local information, which also improves the segmenting accuracy. Shang *et al.* divided the image into key pixels and non-key pixels, and used the key pixels to segment the remaining non-key pixels [42]. This method is called fast fuzzy C-means clustering based on key pixels (FKPFCM). The FKPFCM algorithm performs Gaussian filtering and non-maximum suppression operations before clustering.

Although the above mentioned algorithms achieve good results, there are many other algorithms for image segmentation. Such as patch-based methods divide the image into square regions first, and assign the same label to every pixel in each patch [43]. This algorithm exploits morphological processing to reduce the misclassification phenomenon at the boundaries in the result map [44]. The method of using image patches as processed elements is also widespread in deep learning methods [45]. Moreover, the concept of superpixels has also drawn much attention in the image segmentation literature [46]. Generating more appropriate superpixels can also improve the performance of segmentation [47]. The simple linear iterative clustering (SLIC) algorithm is a commonly used method that generates a certain number of superpixels [48]. It can be used in FCM-based segmentation methods to help reduce the algorithm running time. However, for SAR image segmentation, it is necessary to adjust the SLIC algorithm [49].

In this paper, a new unsupervised SAR image segmentation algorithm, called thumbnail-based hierarchical fuzzy c-means (THFCM), is proposed. The main contributions are as follows:

- In order to improve the segmentation efficiency, the proposed method firstly divides the image into pixel groups, then generates a thumbnail which is much smaller than the original image. That can help reduce the time used for the clustering operation on thumbnail compared with attempting clustering on the entire input image.
- In contrast to other region-based segmentation methods, the proposed method selects the major pixels in the pixel groups, and calculates the mean values to generate a thumbnail. Then it segments the thumbnail using local spatial information. The influence of noisy pixels on the clustering result of the overall region can be reduced.
- To make the segmentation result more uniform and accurate, clustering results of the thumbnail are used to segment the input SAR image hierarchically.

The remainder of this paper is structured as follows. Section II describes the THFCM algorithm in detail. Section III presents the results of empirical experiments to evaluate performance. The variable-controlling method is employed to analyze the sensitivity of the parameters, then the performance of our proposed THFCM algorithm is evaluated in comparison with four other state-of-the-art algorithms. Comparison experiments are preformed using both simulated and real SAR images.

II. Proposed Method

The SAR segmentation task is to assign a proper label for every pixel in the input SAR image, then obtain a segmentation result map $R = \{r_{ij},\ 0 \le i \le M,\ 0 \le j \le N\}$. In this paper, the input SAR image is $X = \{x_{ij},\ 0 \le i \le M,\ 0 \le j \le N\}$, and it can be segmented into C regions. Where x_{ij} represents the intensity value of the pixel at the i-th row and the j-th column.

THFCM works on thumbnails and can improve segmentation efficiency while guaranteeing state-of-the-art segmentation accuracy. The proposed algorithm has three main steps as follows.

(1) Generate the thumbnail

The SAR image is divided into pixel groups through an iterative clustering process. The major pixels are selected according to the intensity histogram of each pixel group. And the pixel value of the thumbnail is obtained by calculating the mean intensity of the major pixels in the corresponding pixel group.

(2) Segment the thumbnail

The FCM algorithm is used to segment the thumbnail, and a regularization term is adopted in THFCM to alleviate the influence of the neighbor pixels [50]. The neighborhood level is used to control the scale of the irregular neighborhood window.

(3) Segment the input SAR image

The major pixels, selected in step (1), are segmented according to the clustering results of their thumbnail. The proposed algorithm gives the corresponding label to the

selected major pixels in every pixel group. Then hierarchical segmentation is performed for the remaining pixels by combining the obtained clustering centers and then a majority voting approach. The flow chart of the method is shown in Fig. 1.

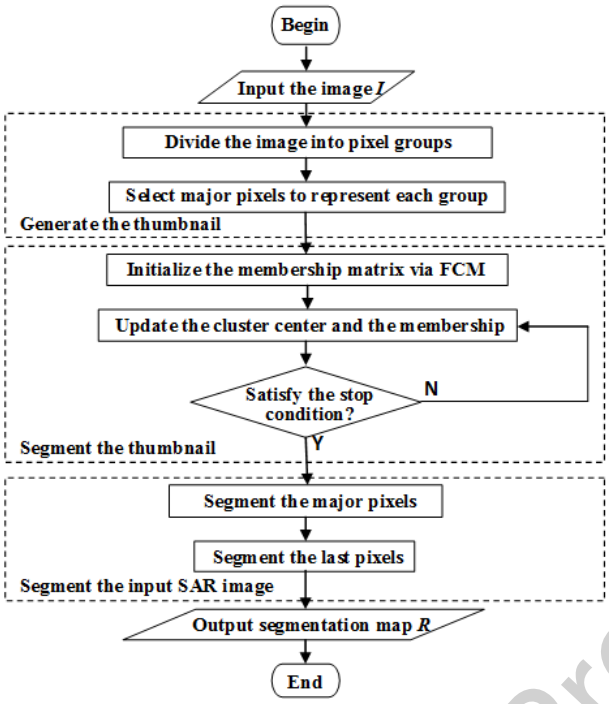

Fig. 1. The flow chart of THFCM.

A. *Generation of the Thumbnail*

The thumbnail is generated to improve the segmentation efficiency, and to suppress the influence of speckle noise. To achieve these effects, the thumbnail needs to satisfy the following requirements. 1) The size of the thumbnail must be significantly smaller than the overall input image. 2) The thumbnail should adequately represents the features of the input image. 3) The thumbnail should be less affected by the speckle noise.

A simple strategy, to generate a low-resolution thumbnail, is that of using the average pooling operation to represent a square patch of pixels by a single pixel. Then clustering is performed on the thumbnail, which is computationally cheaper than clustering the original input image. However, the pixels in each square patch might belong to different regions (different classes). Therefore, adopting a simple regular grid of pixel patches as the clustering unit may result in the loss of some useful information. Many researchers, e.g. SLIC [49], modify the original pixel patches into superpixels, whose boundaries are more consistent with the real edges in the input image. This seems a sensible way to overcome the weakness of regular square pixel patches. Nevertheless, the superpixels in SAR images typically still contain some small regions or discrete pixels, and the SLIC merges them into the neighbor superpixels. That is obstacle for the generation of thumbnail because the locations of superpixels are not regular. In this paper, THFCM divides the input SAR image into feature-similar pixel groups and uses them to generate the thumbnail.

The process of generating feature-similar pixel groups is as follows. Firstly, each pixel x_{ij} is represented by a 9-dimensional eigenvector $\boldsymbol{v}(x_{ij})$, which is composed of intensity values in the 3×3 neighborhood centered on pixel x_{ij}. Next, the input image X is divided into pixel patches in the size of $P\times P$, and each pixel patch forms an initial pixel group. In each pixel group, at each time step, the eigenvector is represented by the average eigenvector of all pixels, and its center position is represented by the average position of all pixels. Next, two steps are performed alternately in each iteration: the allocating step and the updating step.

In the allocating step, the group center of each non-group pixel is searched, and this pixel is allocated to the group center with the most similar intensity in the $S\times S$ neighborhood window, where $S=2P-1$. The distance Δ between the center pixel x_{ij} and its neighbor pixel $x_{i'j'}$ based on the pixel patch is

$$\Delta(x_{ij}, x_{i'j'}) = \| \boldsymbol{v}(x_{ij}) - \boldsymbol{v}(x_{i'j'}) \|^2 . \quad (1)$$

The structure similarity of two pixels can be measured according to this distance. The smaller the Δ, the more similar the two pixels are. After all pixels are allocated to the pixel group, the eigenvector and center position of each pixel group are updated in the updating step, by calculating the average eigenvector and average position of the pixels in the pixel group. The obtained group eigenvector and center position will be used to measure the feature similarity in the allocating step of the next iteration. These two steps are performed in sets of ten iterations alternately, to output the feature-similar pixel groups.

To intuitively illustrate the process of modifying the regular square pixel patches into pixel groups, a 15×15 example image is shown in Fig. 2.

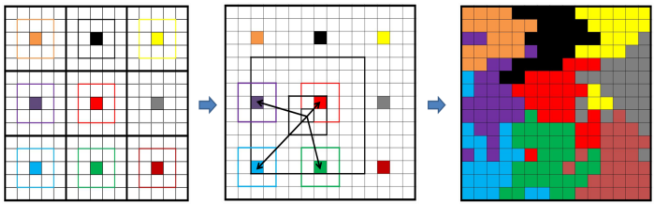

Fig. 2. Schematic diagram of pixel group generating process.

As shown in Fig. 2, the initial patch size $P=5$, and the image of size 15×15 is divided into nine square patches. The central pixel of every regular square patch is used as an initial group center. Nine different colors are used to represent the group centers of each patch. Then, the most similar pixels to the group centers are obtained by equation (1) in the window of $S\times S$ where $S=9$. These are labeled as the same group. After the algorithm converges, the feature-similar pixels are marked the same color in each pixel group. The pseudo-code for the pixel groups generating process is summarized in Algorithm 1.

After the input SAR image is divided into pixel groups, the major pixels are selected from each pixel group to generate the thumbnail. To obtain the major pixels, we establish the intensity histogram for each pixel group. The smallest and largest intensity values are recorded in every group. Then the intensity range is divided into B bins. For each pixel group, major pixels are selected that the bin with the largest number of pixels.

Algorithm1: process of generating pixel groups.

Input: SAR image X, patch size P, the max number of iteration T_G.
Output: pixel groups map R_G
Begin
1. Divide the image X into $P\times P$ regular square patches, and initialize the group centers, set t_G=1;
2. For each pixel except the group centers, calculate the similarity with the group centers in the range of $S\times S$, where S=2P-1;
3. Mark every pixel as the same group as the most similar group center in the range of $S\times S$ around the proposed pixel;
4. Update the gray value of the group centers using the mean intensity of current pixel groups;
5. If $t_G>T_G$, execute step 6; otherwise, $t_G=t_G+1$ and go to step 2;
6. Output the pixel group map R_G.

End

After the major pixels of every group is obtained, the pixel group is represented by mean intensity of these major pixels in this group. So that the size of thumbnail is P times smaller than the original image. Here a real SAR image is adopted as an example, SAR image and obtained thumbnail are shown in Fig. 3(a) and (b). It can be seen that edges in the original image have been preserved in thumbnail.

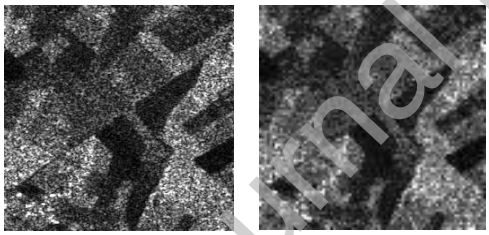

(a) (b)

Fig. 3. Comparison of the original SAR image and the thumbnail. (a) the Input SAR image; (b) Thumbnail.

B. Segmentation of the Thumbnail

In section *A*, we have obtained the thumbnail $S = \{s_{ij}, 1\le i\le m, 1\le j\le n\}$, where $m=\lceil M/P\rceil$, $n=\lceil N/P\rceil$ where m and n are the width and height of thumbnails, M and N are the width and height of input image, P is the patch size. Inspired by ADFLICM [35] and FKPFCM [42], we segment the thumbnail using FCM algorithm with a regularization term, incorporating spatial local information in the thumbnail. That is equivalent to using the spatial non-local information in the input SAR image. The process of generating thumbnail in section *A* uses the spatial local information of the input SAR image. So the proposed method actually combines the spatial information on different scales. In order to maintain the diversity of the neighborhood window, we use an irregular window [50] centered at the central pixel.

The objective function to be minimized is as follows:

$$J=\sum_{i=1}^{m}\sum_{j=1}^{n}\sum_{c=1}^{C}\left(u_{ijc}{}^{f}(s_{ij}-v_c)^2+\sum_{(\tilde{i},\tilde{j})\in W_L} w_{\tilde{i}\tilde{j}}\left(1-u_{\tilde{i}\tilde{j}c}\right)^{f}\left(s_{\tilde{i}\tilde{j}}-v_c\right)^2\right). \quad (2)$$

where s_{ij} is the pixel value at the i-th row and the j-th column in the thumbnail which is also the current central pixel, C is the number of clusters, u_{ijc} indicates the membership degree of the pixel x_{ij} belonging to the c-th cluster, and v_c is the c-th cluster center, f is the fuzzy factor which is usually taken as 2, W_L is the set of all pixels in the L-level neighborhood window of the processed central pixel s_{ij}. The coefficient $w_{\tilde{i}\tilde{j}}$ controls the influence that every neighbor pixel has on the central pixel s_{ij}. The proposed method uses the neighbor pixels on different scales by adjusting the neighborhood level L, which is illustrated in (3) as follows:

$$W_L=\left\{(\tilde{i},\tilde{j})\middle|(i-\tilde{i})^2+(j-\tilde{j})^2\le 2^{L-1}\right\}. \quad (3)$$

We set the neighborhood range as a 9×9 square window centered at the pixel s_{ij}. The pixels outside this area are not considered. Therefore, the possible value of the neighborhood level L is in the set {1, 2, 3, 4, 5, 6}. We show the varying values of neighborhood level for pixels within the maximum area in Fig. 4.

6	6	6	6	5	6	6	6	6
6	6	5	5	5	5	5	6	6
6	5	4	4	3	4	4	5	6
6	5	4	2	1	2	4	5	6
5	5	3	1	s_{ij}	1	3	5	5
6	5	4	2	1	2	4	5	6
6	5	4	4	3	4	4	5	6
6	6	5	5	5	5	5	6	6
6	6	6	6	5	6	6	6	6

Fig. 4. Distribution diagram of the neighborhood level.

As shown in Fig. 4, the darker the color is, the smaller the value of neighborhood level is. After the parameter L is set, all the pixels whose level value is smaller than L are used to segment the central pixel s_{ij}.

The weight $w_{\tilde{i}\tilde{j}}$ in (2) is determined by the similarity between s_{ij} and the central pixel $s_{\tilde{i}\tilde{j}}$. The more similar these two pixels are, the larger the weight $w_{\tilde{i}\tilde{j}}$ is. Then the greater the influence that $s_{\tilde{i}\tilde{j}}$ has on the current center pixel s_{ij}. As shown in (4), the weight $w_{\tilde{i}\tilde{j}}$ is composed of two parts: distance weight w_d and intensity weight w_i.

$$w_{\tilde{i}\tilde{j}}=w_d\times w_i=\frac{1}{(i-\tilde{i})^2+(j-\tilde{j})^2+1}\times\exp\left(-\left|\log\frac{s_{ij}}{s_{\tilde{i}\tilde{j}}}\right|\right), \quad (4)$$

where w_d is determined by the Euclidean distance between the position of central pixel s_{ij} and the corresponding

neighborhood pixel $s_{\tilde{i}\tilde{j}}$. The smaller the distance is, the larger the weight w_d is. Moreover, the weight w_i reflects the similarity between the two pixels in the term of intensity values. The larger the disparity between their intensity values is, the smaller the weight w_i is. These two items evaluate the similarity between these two pixels from different perspectives.

Taking the derivative of the objective function, the update formulas of the membership degree matrix can be obtained and the cluster center vector as follows:

$$v_c^t = \frac{\sum_{i=1}^{m}\sum_{j=1}^{n}(u_{ijc}^t)^f s_{ij}}{\sum_{i=1}^{m}\sum_{j=1}^{n}(u_{ijc}^t)^f}, \tag{5}$$

$$u_{ijc}^t = \frac{1}{\sum_{c'=1}^{C}\left(\frac{\left|s_{ij}-v_c\right|+\sum_{(\tilde{i},\tilde{j})\in W_{ij}} w_{\tilde{i}\tilde{j}}\left(1-u_{ijc}^{t-1}\right)^f\left(s_{\tilde{i}\tilde{j}}-v_c\right)^2}{\left|s_{ij}-v_{c'}\right|+\sum_{(\tilde{i},\tilde{j})\in W_{ij}} w_{\tilde{i}\tilde{j}}\left(1-u_{ijc'}^{t-1}\right)^m\left(s_{\tilde{i}\tilde{j}}-v_{c'}\right)^2}\right)^{1/f-1}}. \tag{6}$$

In each iteration *t*, the membership degree and the cluster centers are updated separately until the algorithm reaches the termination condition. According to the final membership matrix, we give each pixel in the thumbnail the class label corresponding to the maximum membership degree as shown in (7):

$$rs_{ij} = \arg\max_c\left(u_{ijc}\right), c = 1, 2, ..., C. \tag{7}$$

In this paper, In order to make apple-to-apple comparison with other state-of-the-art algorithms, the number of clusters is adopting as same as it in the compared algorithms.

Then the thumbnail segmentation result map is consequently obtained after the defuzzification process. In summary, the process of the thumbnail segmentation is shown in Algorithm2.

Algorithm2: process of the thumbnail segmentation.

Input: the thumbnail *S*, the number of clusters *C*, the max number of iterations *T*, the patch size *P*, the number of histogram bins *B*, the neighborhood level *L*.

Output: the clustering result map of the thumbnail R_s.

Begin

1. Extend the boundary of the *S* and find the neighborhoods in level *L* for every pixel s_{ij}, set the iterative counter t=1;
2. Initialize the membership matrix *U* by FCM;
3. Update the clustering center vector *V* using (5);
4. $t = t + 1$, and update the membership degree matrix *U* using (6);
5. If $t>T$, execute step 6; otherwise, go to *step* 3;
6. Label every pixel in the thumbnail using (7);
7. Output the clustering map R_S.

End

C. Segmentation of the input SAR Image

Some patch-based or superpixel-based image segmentation methods often assign the same result label directly to all the pixels belonging to the patch or superpixel. And the subsequent morphologic processing may be performed on the obtained result map [44]. This approach can loose some detailed information, and it requires that the image resolution is high enough. The reason we use a region to be segmented as a whole is that the pixels in the region are very similar. However, there are always some pixels whose value has a very large disparity with others. These pixels contain not only the seriously noisy pixels but also the edges or boundaries in the input SAR image. Inspired by [42] and [51], we leave these pixels behind and firstly process the major pixels. Then we segment these remaining pixels according to the pre-clustered pixels in their neighborhood window. This approach is also beneficial to obtain a more homogeneous segmentation result map.

In particular, the pixels in the input SAR image need to be traversed three times to complete the final segmentation map.

1) The major pixels of every pixel group: In the process of constructing the thumbnail, we select the major pixels in the pixel groups to calculate the average intensity and average position. When segmenting the input SAR image, the proposed algorithm firstly assigns the obtained pixel group's label to the corresponding major pixels:

$$\begin{cases} r_{ij} = rs_{\tilde{i}\tilde{j}} & \text{if } (i, j) \in S_{\tilde{i}\tilde{j}} \\ r_{ij} = 0 & \text{otherwise} \end{cases}, \tag{8}$$

where, $S_{\tilde{i}\tilde{j}}$ is the set of the major pixels in the input SAR image of the pixel group corresponding to the position $(\tilde{i}, \tilde{j})$ in the thumbnail. The label r_{ij}=0 means that the current pixel has not been segmented in this traversal.

2) Pixels that obtained consistent label through two different approaches: After the first traversal, most of the pixels in the uniform region have been segmented. And the remaining part mainly contains the pixels with complex local structures. According to the fuzzy clustering centers obtained by clustering the thumbnail, a possible label value ra_{ij} can be obtained by comparing the difference between the current pixel and the different clustering centers:

$$ra_{ij} = \arg\min_{1\le c\le C}\left\|x_{ij}-v_c\right\|. \tag{9}$$

In addition, most of the pixels in the neighborhood of the remaining pixels have been given a class label in the first traversal. Since the pixels of the same region tend to gather in a continuous area, we can obtain another possible label value rb_{ij} through the majority voting approach, selecting the label that occurs most frequently in the $P\times P$ window of the current pixel:

$$rb_{ij} = \arg\max_r \left|W_r\right|, \tag{10}$$

where, W_r represents the set of pixels whose label is *r* in the $P\times P$ window centered at the current pixel.

The intuitive interpretation of the majority voting approach is shown in Fig. 5.

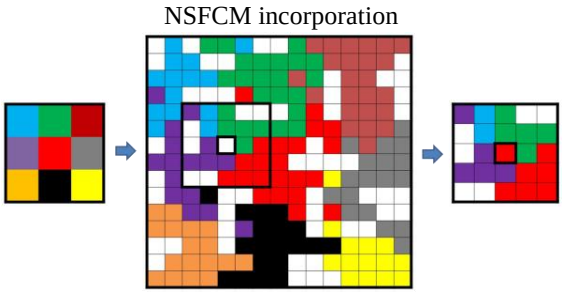

Fig. 5. Schematic diagram of the majority voting approach.

As shown in Fig. 5, after we assign the thumbnail's label to the corresponding major pixels, there are some uncolored pixels remained to the next traversal. Using majority voting approach, we firstly extract the $P\times P$ window centered at the current uncolored pixel, then assign the label that occurs most frequently to it.

If the label obtained by the two approaches is consistent, the label will be assigned to the current pixel. Otherwise, the current pixel can still not be segmented in this traversal:

$$\begin{cases} r_{ij} = ra_{ij} & \text{if} \quad ra_{ij} = rb_{ij} \\ r_{ij} = 0 & \text{otherwise} \end{cases}. \tag{11}$$

3) The final remaining pixels: After the second traversal, the remaining pixels are mainly discrete noisy pixels. For these pixels, we perform a majority vote operation again according to the results of the previous two traversals to determine the labels of the remaining pixels. In this way, the original SAR image segmentation result map R has been completely obtained.

In summary, we have completed the segmentation process of the input SAR image. Here we show the pseudo-code of the algorithm THFCM in **Algorithm 3**.

Algorithm3: process of THFCM.

Input: SAR image X, segmentation class number C, patch size P, the number of histogram group B, neighborhood level L, the max number of iteration T.

Output: final segmentation map R.

Begin

1. Divide the image X into pixel groups and find the major pixels;
2. Construct the thumbnail using the method in Algorithm1;
3. Segment the thumbnail using the method in Algorithm2 and obtain the thumbnail clustering map R_S;
4. Label the major pixels using R_S;
5. Label the remaining pixels using the method in section C;
6. Output the segmentation map R.

End

III. Experimental Results and Analysis

In this section, THFCM is performed in two simulated SAR images and four real SAR images separately. In order to show the effectiveness of the proposed algorithm in terms of segmentation accuracy and operating time, four state-of-the-art FCM-based SAR image segmentation methods is adopted named CKSFCM [39], NSFCM [40], ALFCM [41], and FKPFCM [42], and one semi supervised deep learning algorithm called SRDNN-MD [51] for comparison and analysis.

A. Experimental images

In order to observe and evaluate the segmentation results of THFCM, simulated SAR images which obtain by adding multiple speckle noise of 1, 2, 4, and 6 looks to the standard images are chose as the input data [52, 53]. The 1-look images of the selected simulated SAR images and their ground truth map are shown in Fig. 6(a)-(d).

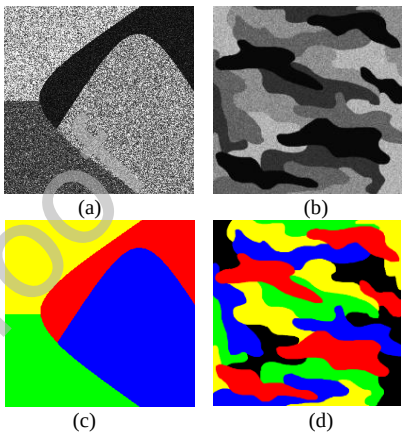

Fig. 6. Simulated SAR images. (a) 1-SI1; (b) 1-SI2; (c) Ground truth map of SI1; (d) Ground truth map of SI2.

SAR systems often perform multi-look processing on images, the larger the number of looks, the less the image is affected by the speckle noise, the higher the image quality is [53]. In order to observe the segmentation results of the proposed algorithm, the images we select are different in the size, the number of clusters, the intensity values of cluster centers and so on. The detailed information of the two simulated SAR images is shown in Table I.

TABLE I Relevant Information of the Simulated SAR Images

	Size	Clusters	Looks	Intensity values
SI1	256×256	4	1,2,4,6	30,92,184,255
SI2	1000×1000	5	1,2,4,6	10,60,120,180,255

As shown in Table I, SI1 is a 4-cluster simulated SAR image in a size of 256×256. The original standard image sets higher intensity values for the four cluster centers. The gap among each cluster are small and it is convenient for a pixel to obtain a similar value with another neighbor cluster after adding artificial noise. SI2 is a larger image whose size is 1000×1000. The size of SI2 increases significantly compared with SI1, and its cluster number changes to 5. The gap among the various cluster centers' intensity value becomes smaller. SI2 is more greatly affected by noise because the speckle noise is a typical multiplicative noise. And the brighter area usually has a greater range of fluctuation. We perform experiments on the two different simulated SAR images.

Moreover, we also use three real SAR images to observe the segmentation results of the proposed THFCM algorithm and the other comparison algorithms. The three real SAR images we selected is shown in Fig. 7(a)-(c).

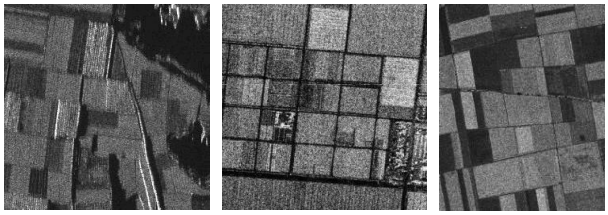

(a) (b) (c)

Fig. 7. Real SAR images. (a) XIAN; (b) MARICOPA; (c) NORDLINGER.

Fig. 7(a) shows the first real SAR image, called XIAN, was taken in the X-band by TerraSAR viewing Xi'an, China, at a resolution of 1 meter. The size of image XIAN is 256×256, This dataset can be divided into three different regions containing different crops. Fig. 7(b) shows the second real SAR image named MARICOPA, imaged in the Ku-band and VV polarization, located at the Maricopa Agricultural Center near Arizona. The size is 350×350 and the resolution is 1 meter. This image can be segmented into 4 classes including three different kinds of XIAN and water area. The third image shown in Fig. 7(c) is called NORDLINGER with the original resolution of 1 meter, HH polarization and in X-band. It was captured by TerraSAR-X, situated in the middle of the Swabian Jura, the Nördlinger Ries. When the image is segmented, the class number is set to be 4.

B. Comparison Algorithms and Evaluation Indicators

In order to verify the effectiveness of the proposed method THFCM on SAR images segmentation problem, in this section we use four state-of-the-art comparison algorithms including the immune clone clustering algorithm based on non-local mean (CKSFCM) [39], the non-local fuzzy clustering algorithm with between-cluster separation measure (NSFCM) [40], the fuzzy clustering algorithm based on adaptive local information (ALFCM) [41] and the fast SAR image segmentation algorithm based on key pixels (FKPFCM) [42]. As illustrated in section I, CKSFCM firstly uses the immune clone algorithm to initialize the clustering centers, then adds non-local information to the clustering process to overcome the effect of speckle noises. NSFCM incorporates the non-local spatial information obtained using an improved non-local mean method and introduces a fuzzy between-cluster variation term into the original objective function ALFCM combining the information of region level and pixel level to perform fuzzy clustering. Region-level local information is used to adaptively control the range and strength of interactive pixels. FKPFCM selects key pixels from the image and clusters the key points first. Then it processes the last non-key points by the key points' clustering results. In addition, using pixel patches to construct thumbnail can also achieve good results. That means, after we divide the image into regular square patches, the major pixels are selected in every patch directly to construct the thumbnail. We called this method patch-based hierarchical fuzzy C-means algorithm (PHFCM), which is also tested as a comparison algorithm.

In order to evaluate the performance of the algorithms, we select the segmentation accuracy (SA) and algorithm running time (Time) as the evaluation indicators. The segmentation accuracy is the percentage of the correctly segmented pixels in the segmentation result map compared to the ground truth map, which is calculated by

$$SA = \frac{\sum_{i=1}^{M}\sum_{j=1}^{N} 1\left(R_{ij} = G_{ij}\right)}{MN}, \tag{12}$$

where $1(\bullet)$ is an indicator function whose value is 1 if and only if the expression between the brackets is real, and 0 otherwise. R_{ij} and G_{ij} severally represent the segmentation result label obtained by the algorithm and the real ground truth label of the pixel x_{ij} in the input SAR image.

C. Parameters analysis

In the proposed methods, the size of pixel patches P, the number of histogram bins B, and the neighborhood level L need to be adjusted. Here we select the simulated image 2-SI1 to analyze the parameters of THFCM, observe and record the influence of these parameters on segmentation accuracy and algorithm running time.

1) Pixel patch size P: The size of pixel patches P determines the reduction ratio of the thumbnail relative to the input SAR image. Intuitively, the larger the pixel patch size P is, the smaller the size of the resulting thumbnail, and the less the algorithm's running time used for clustering. However, as P increases continuously, more and more pixel information will be obscured by the averaging operation, which can also have adverse effects on the algorithm's results.

Here we fix the other two parameters B=3, L=1, for the PHFCM and THFCM and just adjust the parameter P in the set {3, 5, 7, 9, 11, 13, 15}. Then run the proposed algorithms for 10 times setting every selected value of P and calculate the average results to observe and record how the segmentation accuracy (SA) and algorithm running time (Time) change with P constantly increases.

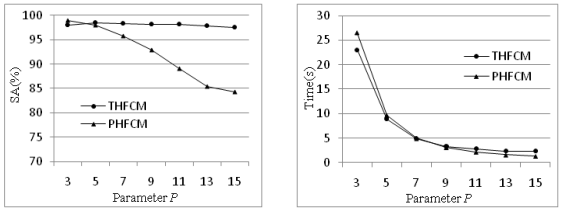

(a) (b)

Fig. 8. The effect of pixel patch size P on PHFCM and THFCM. (a) Segmentation accuracy; (b) Running time.

From Fig. 8, we can see that with the increase of the pixel patch size P, the running time of both algorithms is gradually reduced. But meanwhile, the segmentation accuracy of the algorithms is also decreasing constantly. Fig. 8(a) compares

the decreasing trend of the segmentation accuracy of PHFCM and THFCM with the increase of pixel patch size *P*. It can be seen that the running time of the two methods changes in a similar rate, but the segmentation accuracy of PHFCM decreases more quickly than that of THFCM. That means the sensitivity of the proposed THFCM to parameter *P* is reduced, so that we can increase the pixel patch size *P* as much as possible to further shorten the algorithm running time under the premise of ensuring the segmentation accuracy.

2) Neighborhood level L: During thumbnail segmentation process, the neighborhood level *L* controls the scale of the neighborhood information in the thumbnail. For different images, we need to adjust *L* to control the use of the local and non-local information. When processing a central pixel, the intensity information of the adjacent or nearby pixels can also be used to reduce the influence of noises. However, if we consider the pixels in a very large window, some important details can be neglected.

Here we fix the other two parameters $P = 5$ and $B = 3$ for the proposed algorithm THFCM, and let *L* take the values of the set {1, 2, 3, 4, 5, 6} in proper order. For each value we run the proposed THFCM algorithm independently for 10 times to obtain the average results, record the segmentation accuracy (SA) and algorithm running time (Time) with *L* changing. The test results are shown in Fig. 9. From the experimental results in Fig.9, we can see that the neighborhood level *L* is another important parameter that affects the running time of the algorithm. As *L* increases, the algorithm needs to utilize the pixel information in a larger range and spend more calculation time on clustering operation. For the tested image, we obtain the largest segmentation accuracy when L=1. And the SA's change range is not very large within a range of about 1.5 percent, which means that the proposed THFCM algorithm has nearly stable performance when *L* changes.

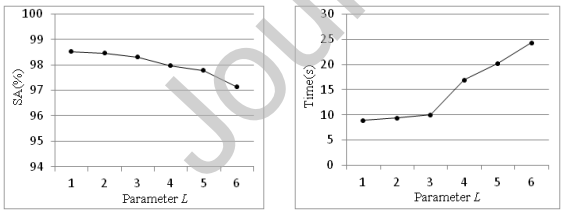

(a) (b)

Fig. 9. The effect of neighborhood level *L* on THFCM. (a) Segmentation accuracy; (b) Running time.

3) Histogram groups number B: When selecting the major pixels to generate the thumbnail, we construct the intensity histogram and the quantity of pixels in each intensity value range needs to be counted. The number of histogram bins *B* directly affects the quantity of selected major pixels. If *B* is small, most of the pixels in a pixel group may concentrate in one intensity bin and be selected as the major pixels. Otherwise, the algorithm will leave more pixels to be segmented in the next traversal. To show that, we also record the number of pixels that are left to the next traversal, which is represented by "LPN" in Fig. 10.

Here we fix the other two parameters $P = 5$, $L = 1$, let *B* take the values in the set {3, 5, 7, 9, 11, 13, 15} in a proper order. For each value we run the proposed THFCM algorithm independently for 10 times. We record the segmentation accuracy (SA), the algorithm running time (Time) and the number of last pixels (LPN) in the Fig. 10 as *B* changes.

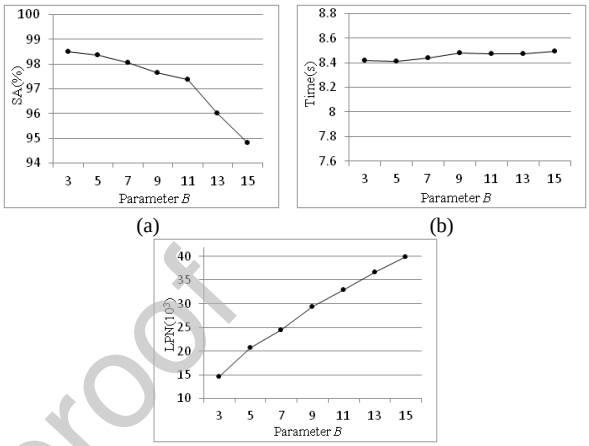

(a) (b)

(c)

Fig. 10. The effect of histogram group number *B* on THFCM. (a) Segmentation accuracy; (b) Running time; (c) Last pixels' number.

As shown in Fig. 10, as the number of histogram bins increases, the quantity of last pixels becomes larger and larger, and meanwhile the segmentation accuracy decreases constantly. The size of image SI2 is 256×256, which contains 65536 pixels. When we set the parameter *B* as the smallest value "3", the number of last pixels is 14555, which means nearly 20 percent of all the pixels are left to the second layer for segmentation. When *B* takes the largest value B=15, there are more than 50 percent, 39958 pixels left, and we obtain a bad result because of excessively ignoring the useful image information. Fig. 10(c) shows that the running time stays almost stable within the change range less than 0.1s, which means that the parameter *B* has small effects on the running time of THFCM.

In summary, increasing the segmentation accuracy and decreasing the algorithm's running time are two different aspects in the task of improving the algorithm performance. The experimental results show that we have reduced the sensitivity of the modified algorithm THFCM to the parameters. That enables the algorithm to further shorten the algorithm running under the premise of ensuring the segmentation accuracy.

D. Computational Complexity Analysis

In the above parameter analysis section, we have analyzed the variety of the algorithm running time while the parameter *P*, *L*, or *B* is changing. Except for these parameters, the size of the input SAR image is also a decisive factor for computational complexity. We assume that the input SAR image has *D* pixels. To show the influence of these

parameters on the algorithm running time, we use D, P, L and B to represent the computational complexity. The time complexity of the thumbnail generating process is O(D). And we obtain a thumbnail that has N/P^2 pixels. So the time complexity of the thumbnail segmenting process is $O(DN_L/P^2)$, where N_L is the number of used neighbor pixel when the neighborhood level is L. Finally, the time complexity of the input SAR image segmenting process is O(D). It is intuitive that generating thumbnails can reduce the time spent on clustering.

E. Experimental conditions

All the experiments were executed in MALAB R2017a environment, using a computer with an Intel core i5 3.30-GHz CPU and 8-GB RAM. In order to show the effectiveness of the proposed THFCM, firstly we select two simulated SAR images and three real SAR images. For the two simulated SAR images, the parameters of THFCM are set as follows: The parameter P is 5 for every simulated SAR image. And the parameter B is 3 for every simulated SAR image. The parameter L is 3 for all the simulated images except the two 1-look images: for 1-SI, L=4, for 1-SI2, L=2. For the three real SAR images, the parameters of THFCM are set as follows: for XIAN, P=5, L=3, B=5; for MARICOPA, P=3, L=1, B=3; for NORDLINGER, P=3, L=2, B=7. Furthermore, to observe the running time, the max number of iteration T is set as 100 for every image. Our experimental results confirm that the proposed method generates good segmentation results by using these choices of parameters.

F. Results and analysis on simulated SAR images

In order to observe the experimental results, we show the segmentation result maps of each method and record the segmentation accuracy and the running time.

FCM algorithm and its series of varieties have a problem that they are sometimes sensitive to the randomly set initial condition. That can make the algorithm converge to the local optimum. During our experiments, it is also found that some algorithms obtain fluctuant results under different initial conditions, especially when segmenting the simulated SAR images in lower look. That is because the gap among every cluster center is too small. There are some runs in which the algorithms obtain a very low segmentation accuracy because of a whole region misclassification phenomenon. Therefore, except the segmentation accuracy and the running time, we also record the number of times that the algorithm obtains higher segmentation accuracy as the effective number in the 20 runs, which is represented by "EN" in the following tables. That can reflect whether the algorithm can reduce the dependency on the initial conditions. In addition, the statistical segmentation accuracy and running time in the following results are calculated by the mean value or better results of 20 runs. Similarly, we select the representative better segmentation result maps of the algorithms in the EN runs of 20 as shown in the following figures.

1) Results and analysis of SI1: The simulated SAR image SI1 can be segmented into four classes, corresponding to the four different intensity values shown in Table I. The obtained segmentation maps of 2-SI1 are shown in Fig. 11(a)-(f).

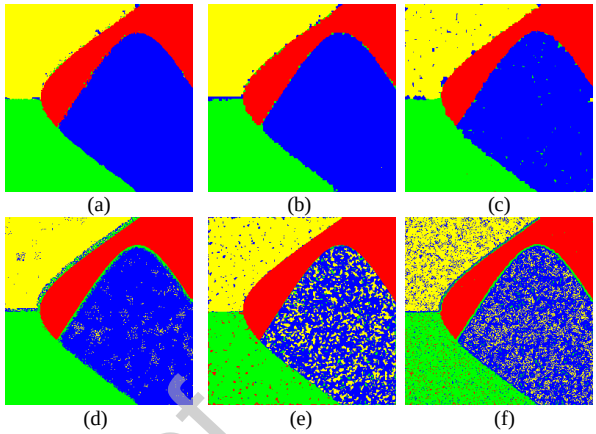

Fig. 11. Segmentation result maps of the six algorithms on 2-SI1. (a) THFCM; (b) PHFCM; (c) FKPFCM; (d) NSFCM; (e) ALFCM; (f) CKSFCM.

Fig. 11 shows that each algorithm can segment the image into four regions, but all methods have different degrees of misclassification phenomenon. The inherent speckle noise of SAR image is a typical multiplicative noise, and the brighter regions in the image are more affected by that. From our experimental results, it can also be seen that each algorithm has the misclassification regions mainly in the brighter areas, which is represented by yellow. Compared with the other comparison algorithms, ALFCM obtains the clearest boundaries. However, its misclassification regions also cover a large proportion in the segmentation result map (Fig. 11(e)). The FKPFCM reduces the discrete misclassified pixels in a great degree (Fig. 11(c)). The result maps of NSFCM and CKSFCM are not ideal enough at the boundary regions.

The PHFCM algorithm significantly reduces the number of discrete misclassified pixels in the segmentation map. That makes the results more homogeneous and improves the segmentation accuracy (Fig. 11(b)). However, compared with the modified method THFCM, the boundary in the result map of PHFCM is not clear enough. In particular, the boundary between the yellow and green region produces a patch-level mismatch phenomenon. As shown in Fig. 11(a), THFCM obtains a result map that is more consistent with the boundaries and details because of the modification operation of the pixel groups.

To observe the results more intuitively, Table II compares the segmentation accuracy (SA) and the running time (Time) of each algorithm. It can be seen that the proposed THFCM algorithm not only has the advantages of segmentation accuracy, but also reduces the running time of the algorithm. That is because the algorithm performs clustering only on the thumbnails rather than all the image pixels. And as it is illustrated in the parameters analysis section, the modified method THFCM is more effective than PHFCM. We can increase the pixel patch size P as much as possible to further

shorten the running time under the premise of ensuring the qualified segmentation accuracy. As shown in Table II, when segmenting the image 6-SI1, PHFCM obtains the highest segmentation accuracy, but its running time is not very ascendant among all the algorithms. That is because we set the patch size P=3, which is the smallest available value that we can select. The proposed THFCM uses the shortest running time on every image, and the segmentation accuracy is almost the highest.

TABLE II RESULTS ON THE SIMULATED IMAGES OF SI1

Algorithms	1 look			2 looks			4 looks			6 looks		
	EN	SA(%)	Time(s)	EN	SA(%)	Time(s)	EN	SA(%)	Time(s)	EN	SA(%)	Time(s)
CKSFCM	20	65.77	367.26	20	82.37	174.64	20	86.63	99.21	20	89.89	71.87
NSFCM	20	87.80	25.83	15	92.94	25.86	18	96.66	25.87	16	97.92	25.85
ALFCM	0	42.43	51.76	20	86.54	33.69	20	94.57	23.05	20	97.79	14.55
FKPFCM	20	96.47	24.27	20	97.98	26.86	19	98.53	24.43	18	98.60	23.97
PHFCM	20	97.23	34.02	20	98.42	33.52	20	98.54	33.10	20	**98.79**	32.92
THFCM	20	**97.43**	**16.74**	20	**98.51**	**8.62**	20	**98.59**	**8.56**	20	98.67	**8.51**

Through Table II we can see that when performing the ALFCM algorithm on the 1-look images, we always obtain a very low segmentation accuracy. So the ALFCM algorithm is limited when segmenting the images seriously affected from speckle noise. But ALFCM has another advantage that as the number of looks increases, the convergence rate of ALFCM becomes higher and higher. The CKSFCM algorithm spends the longest running time on the segmentation of SI1 because of its initialization operation. Moreover, the best result is obtained on 6-SI1 of each algorithm comparing that on other three looks. So that we can summarize out that the more seriously the image is affected by the noise, the disparity among the algorithms' effects.

In addition, the FCM algorithm and its varieties are sometimes sensitive to the random initial conditions. So that the segmentation accuracy of some algorithms may fluctuate greatly in different runs. For this processed image, FKPFCM algorithm has a high segmentation accuracy and the running time of it is also superior among the algorithms. But because the gap among the intensity value of different cluster centers is very small, there are a small number of low accuracy results among the 20 operations of FKPFCM. These runs are not included in the average operation used to obtain the results in Table II. The method NSFCM obtain more fluctuate results than FKPFCM, although it can also create good results in most efficient runs of the 20. The proposed methods PHFCM and THFCM reduces the possibility of this phenomenon and obtain more stable segmentation results.

2) Results and analysis of SI2: Except the above small-scale simulated image, we also need to observe the segmentation results on a larger image. The size of SI2 is 1000×1000, which is much larger than SI1. In addition, we choose five different intensity values for five clustering centers in SI2. That also makes the differences among every region become smaller. The SI2 images are affected by the speckle noise more seriously. And the boundaries in SI2 are more complicated, which requires greater segmentation performance. We show the segmentation result maps on the image 2-SI2 in Fig. 12(a)-(h).

From Fig. 12 we can see that the yellow region is still the easiest misclassified one and all the algorithms have some discrete wrong pixels there. Fig. 12(d) shows that the result of NSFCM is qualified and the segmentation map is more homogeneous than the other comparison algorithms, but the boundaries is not clear enough. It can be seen in Fig. 12(b) that THFCM can obtain a very homogeneous segmentation result map with nearly no discrete misclassified pixels. But in the same way as SI1, there are a large quantity of pixels that are segmented into the third type at the boundaries of two different colors. This is because the algorithm performs averaging operation on the pixels belonging to different regions while segmenting some of the pixels around boundaries. However, the proposed THFCM algorithm adjusts the edge of the pixel patches and modifies the pixel patches into pixel groups that are more consistent with the image details. So that the THFCM algorithm achieves great improvement at the boundary under the premise of a certain degree of uniformity (Fig. 12(a)). This image has a larger size, and the running time of these six algorithms has many differences. Similarly, we give the concrete results in Table III.

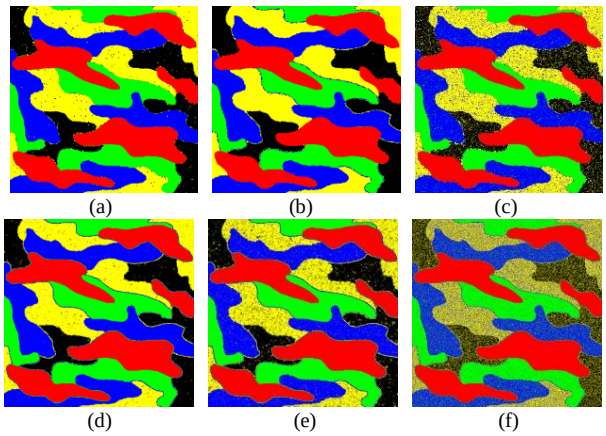

Fig. 12. Segmentation result maps of the six algorithms on 2-SI2: (a) THFCM; (b) PHFCM; (c) FKPFCM; (d) NSFCM; (e) ALFCM; (f) CKSFCM.

Table III shows that although the images are more complex, the segmentation accuracy of each algorithm has improved compared with the previous SI1. This is because the image size becomes larger, the number of pixels in the homogeneous area increases more greatly than that of boundary area, so that the segmentation accuracy values increase. However, these indicators can still reflect the segmentation effects of different algorithms on the same image. We can see that when segmenting 1-SI2, both the CKSFCM and ALFCM obtain a low segmentation accuracy. The result map of CKSFCM algorithm has many discrete misclassification pixels so that

result is not very good, while the result of ALFCM is even worse because there is a whole region being wrongly segmented. In addition, although the PHFCM algorithm obtains nearly the most homogeneous segmentation result map, it also has the whole region misclassification phenomenon when segmenting 1-SI2, the THFCM algorithm more effectively avoids this situation from occurring.

TABLE III RESULTS ON THE SIMULATED SAR IMAGES OF SI2

Algorithms	1 look			2 looks			4 looks			6 looks		
	EN	SA(%)	Time(s)	EN	SA(%)	Time(s)	EN	SA(%)	Time(s)	EN	SA(%)	Time(s)
CKSFCM	20	69.58	3210.54	20	81.67	3044.16	20	88.04	1934.51	20	91.34	1581.54
NSFCM	20	92.77	1016.17	20	95.63	1009.27	20	96.38	1011.72	20	96.77	1011.94
ALFCM	0	67.10	8241.84	20	81.68	2065.32	20	92.37	978.43	20	92.46	533.26
FKPFCM	20	96.59	839.31	17	97.44	856.80	19	97.99	861.36	15	98.18	926.52
PHFCM	11	96.01	474.64	20	97.72	470.71	20	98.03	469.11	20	98.12	467.57
THFCM	20	**97.08**	**161.18**	20	**97.92**	**153.02**	20	**98.25**	**152.80**	20	**98.38**	**153.01**

In summary, the above experimental results prove that the proposed PHFCM and THFCM algorithms obtain the best segmentation results in terms of segmentation accuracy, running time, and algorithm stability for the simulated SAR images selected in this paper.

G. Results and analysis on real SAR images

The performance of the algorithms needs to be tested in practice. We apply the proposed algorithms and a series of comparison algorithms to the real SAR images illustrated in the previous section A. In order to visually observe the segmentation performance of each algorithm, we show the segmentation result map of each algorithm separately for comparison and analysis. Then at the end of this section, we list the segmentation accuracy and the running time for each method in one table. According to the land types of every real SAR image, the cluster numbers in the proposed methods for the three images named XIAN, MARICOPA and NORDLINGER are separately set as 4.

1) Results and analysis of XIAN: The first real SAR image is named XIAN as shown in Fig. 13(a). It has four different regions, which are respectively marked by four different colors named yellow, red, blue, and green in the ground truth map (Fig. 13(b)). In addition, the segmentation result maps of the proposed THFCM algorithm and the five comparison algorithms are respectively presented in Fig. 13(c)-(h).

As shown in Fig. 13(a)-(h), the yellow region in the image XIAN is easier to be misclassified than any other regions in different colors. The algorithm FKPFCM only mark a small part of yellow region pixels (Fig. 13(e)), while the comparison algorithm NSFCM wrongly segment many pixels that are supposed to be marked in blue into the yellow region (Fig. 13(f)). The obtained position of each region through the algorithm ALFCM and CKSFCM is roughly accurate, but there are still too many discrete misclassified pixels that are wrongly segmented, which makes the segmentation result maps of these algorithm not homogeneous and accurate enough (Fig. 13(g)-(h)). Fig. 13(d) shows that the PHFCM algorithm obtains a more accurate segmentation result map compared to the other comparison algorithms, but there are still some unfaithful squared boundaries in it. This is because it uses regular square pixel patches for clustering, which reduces the information of the boundary areas by the averaging operation. Then as shown in Fig. 13(c), the proposed THFCM algorithm reduces the appearance of gridding edges through generating pixel groups with similar sizes and makes the segmentation map more consistent to the ground truth map of XIAN.

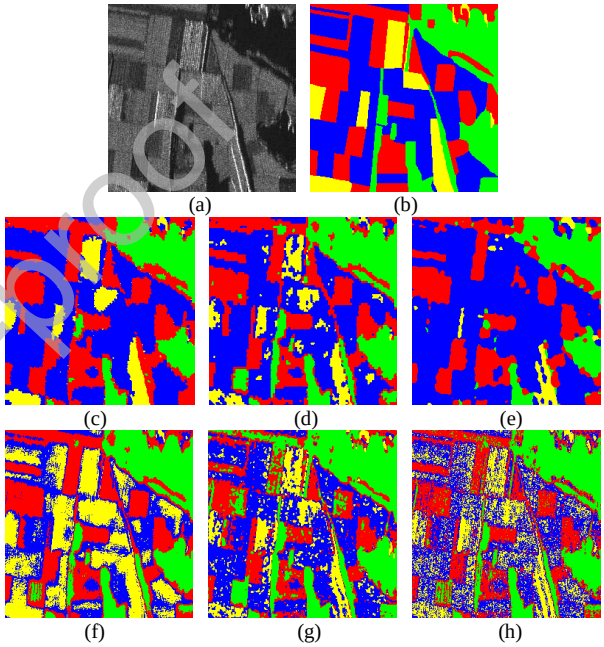

Fig. 13. Segmentation result maps of the six algorithms on XIAN: (a) XIAN; (b) Ground truth map of XIAN; (c) THFCM; (d) PHFCM; (e) FKPFCM; (f) NSFCM; (g) ALFCM; (h) CKSFCM.

2) Results and analysis of MARICOPA: Then we show the results that we use the six algorithms to segment the second real SAR image called MARICOPA, which has four different regions marked by red, blue, green and yellow. Fig. 14(a) and Fig. 14(b) separately shows the image MARICOPA and its ground truth map. And we use Fig. 14(c)-(h) to show the segmentation result maps of the proposed methods and the comparison algorithms in a certain order.

The different regions of MARICOPA images are easy to be confused. As shown in Fig. 14(g) and Fig. 14(h), the ALFCM algorithm and CKSFCM algorithm cannot basically obtain a clear and homogeneous yellow area. The green regions actually take a small proportion in the ground truth map. But many of the comparison algorithms obtain more green pixels in the other regions. In addition, all the methods fail to segment out the blue region completely, which can contain some linear structures in the image.

As shown in Fig. 14(c)-(d), although there are also some misclassified discrete pixels in our results, the four regions are

still clearly distinguished from each other by PHFCM and THFCM. Comparing the two algorithms, the PHFCM algorithm obtain more clear blue details which can be some linear structures, but the result map of THFCM is more homogeneous than that of PHFCM.

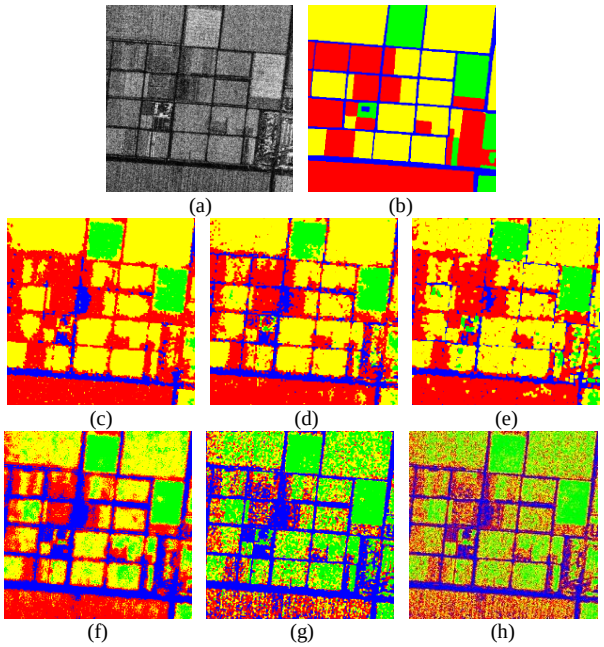

Fig. 14. Segmentation result maps of the six algorithms on MARICOPA: (a) MARICOPA; (b) Ground truth map of MARICOPA; (c) THFCM; (d) PHFCM; (e) FKPFCM; (f) NSFCM; (g) ALFCM; (h) CKSFCM.

3) Results and analysis of NORDLINGER: Next we use the third real SAR image called NORDLINGER to show the performance of the two proposed methods and the four comparison algorithms. As illustrated in Fig. 15(a) and Fig. 15 (b), the image NORDLINGER has four different regions, colored in yellow, blue, green and red. Similar with the previous sections, we show the segmentation result maps of the six algorithms in Fig. 15(c)-(h).

As shown in Fig. 15(e)-(h), the algorithm FKPFCM obtains the most homogeneous segmentation map among the comparison algorithms, but it fails to segment out a part of the green region, which contains some very thin lines. At this respect, the green region in the result of NSFCM is more complete, but it has too many discrete misclassified areas and the yellow region is not clear enough (Fig. 15(f)). As shown in Fig. 15(g)-(h), the algorithms ALFCM and CKSFCM are more seriously affected by this phenomenon so that they can hardly obtain a homogeneous blue region.

Comparing the proposed two methods, the THFCM segment out the green region more completely. And the segmentation result maps obtained by them are more accurate and homogeneous than other comparison algorithms.

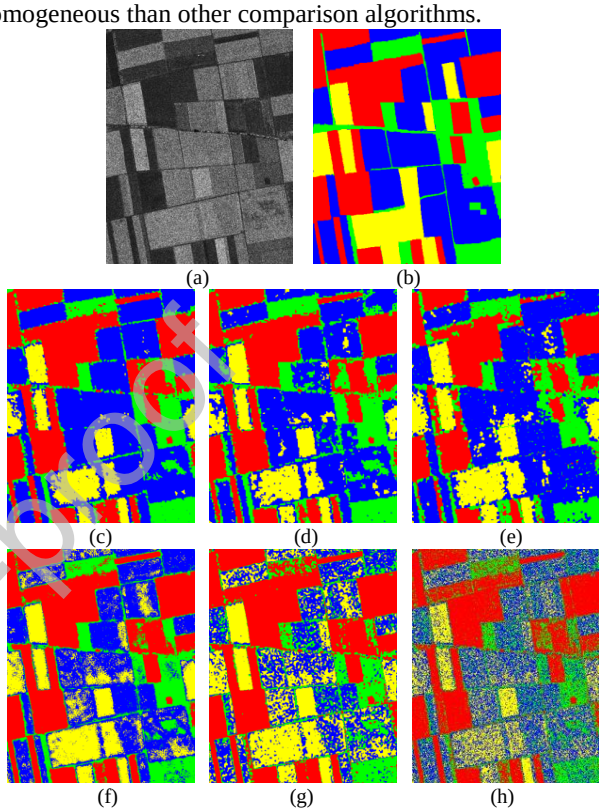

Fig. 15. Segmentation result maps of the six algorithms on NORDLINGER: (a) NORDLINGER; (b) Ground truth map of NORDLINGER; (c) THFCM; (d) PHFCM; (e) FKPFCM; (f) NSFCM; (g) ALFCM; (h) CKSFCM.

4) Statistical results and analysis: To observe and analyze the performance more intuitively, we give the specific results containing the segmentation accuracy (SA) and algorithm running time (Time) in Table IV.

TABLE IV RESULTS ON THE REAL SAR IMAGES

Algorithms	XIAN		MARICOPA		NORDLINGER	
	SA(%)	Time(s)	SA(%)	Time(s)	SA(%)	Time(s)
CKSFCM	71.57	263.65	54.52	435.48	64.81	702.64
NSFCM	65.43	34.06	64.87	54.90	79.73	90.36
ALFCM	74.49	56.25	58.50	113.22	67.04	271.13
FKPFCM	73.73	25.54	68.80	50.68	77.75	92.05
PHFCM	75,93	30.62	72.52	57.58	80.05	93.03
THFCM	**78.52**	**9.16**	**72.66**	**40.16**	**83.98**	**70.04**

Table IV shows the segmentation accuracy of the four real SAR images and the algorithm running time of the proposed algorithm and the comparison algorithms separately. We can see that as the same as the simulated image segmentation results, the algorithm CKSFCM takes the longest time because it uses an immune clone algorithm to initialize the cluster centers. FKPFCM has a certain degree of superiority in both segmentation accuracy and running time. The algorithm FKPFCM proposes an idea of selecting key pixels and combines the non-local information to cluster them, which spends shorter time on clustering operation. In addition, it

ignores some pixels when clustering, which makes the segmentation result map more homogeneous.

Both the proposed PHFCM and THFCM have a dominant performance on three real SAR images. The segmentation accuracy of these two is almost the highest among the six algorithms. But the THFCM has more impressive superiority in terms of algorithm running time. The thumbnails obtained by the two algorithms are both smaller than the original images by several times, which can be determined by the parameter *P*. The algorithm THFCM can further shorten the running time because it modifies the pixel patches into pixel groups which are more consistent to the boundaries in the original images.

Moreover, the robustness of the proposed method needs to be tested by executing several times. We run the THFCM for 100 times on every real SAR image. And the best, mean, worst and variance values of the segmentation accuracy (SA) and algorithm running time (Time) are shown in Table V.

TABLE V ROBUSTNESS ANALYSIS ON THE REAL SAR IMAGES

Images	SA(%)				Time(s)			
	best	mean	worst	variance	best	mean	worst	variance
XIAN	78.56	78.52	78.48	4.23e-08	9.21	9.26	9.32	6.32e-04
MARICOPA	72.77	72.68	72.52	4.52e-07	39.18	39.57	39.86	0.01
NORDLINGER	84.23	84.04	83.89	1.69e-06	67.91	68.39	70.40	0.27

Table V shows that during the 100 runs, the segmentation accuracy and running time have very small fluctuations. The gap are small between the best and worst values and the variance values are very small. That means that the proposed THFCM has a stable performance with different values of the random initial solutions for the algorithm.

H. Comparison with semi supervised deep learning algorithm SRDNN-MD on XIAN dataset

There are many deep learning methods have achieved a great success in image segmentation. These methods, however, are supervised or semi supervised. The proposed algorithm is unsupervised. In order to prove the performance of our algorithm, we compared it with semi supervised deep learning algorithm SRDNN-MD in [51] on XIAN dataset. The result map of the proposed THFCM and the compared method is shown in Fig. 16(a) and Fig. 16(b) respectively.

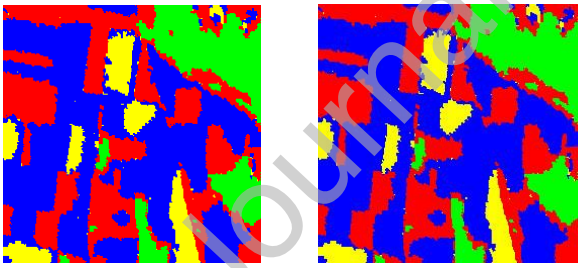

(a) (b)

Fig. 16. Segmentation result maps of the two algorithms on XIAN: (a)THFCM; (b) SRDNN-MD.

It can be seen from the result map that THFCM and SRDNN-MD have obtained the similar result. Both of them can segment the edge well and retain the homogeneity of each region. Compared with the middle part of the two figures, there are less noise in Fig. 16(b), however, the performance of edge segmentation of SRDNN-MD is almost the same as THFCM. The detailed results are shown in Table VI.

TABLE VI RESULTS ON THE REAL SAR IMAGES

Dataset	THFCM		SRDNN-MD	
	SA(%)	Time(s)	SA(%)	Time(s)
XIAN	78.52	**9.16**	**79.61**	549.07

As indicated in Table VI, the segmentation accuracy of SRDNN-MD is 79.61%, which is 1 percentage point higher than that of our algorithm 78.52%, but the time-consuming of this algorithm 549.07 is much higher than that of our algorithm 9.16. This prove the contribution of our methods that thumbnail is introduced as the basis of preliminary segmentation, thus, the proposed algorithm can maintain a comparable segmentation accuracy while improving segmentation efficiency.

In summary, compared with the simulated SAR images, the real SAR images can more accurately reflect the effectiveness of different segmentation algorithms because of their broader extent and more complex land types. And for different number of looks dataset, increasing the number of looks benefits SAR image segmentation accuracy. However, it can be known from the result map of XIAN and NORDLINGER in Fig. 13 and Fig. 15, for different input data, the regular degree of edge also has a great influence on segmentation results. The results show that reduce the influence of speckle phenomenon during the segmentation process can improve the efficiency of solving the problem. The above experiments and results show that the proposed THFCM algorithm have a certain degree of superiority in terms of both the segmentation accuracy and the algorithm running time.

I. Simulation results on ground truth with speckle noise

In order to provide a fair test for all algorithms, the speckle noise with the statistical model of Gaussian distribution is added to the ground truth of 1 look simulated SAR dataset 1-SI1. Fig. 17 (a) and (b) show the ground truth and the added speckle noise with the mean and variance are 0 and 0.01 of 1-SI1 respectively.

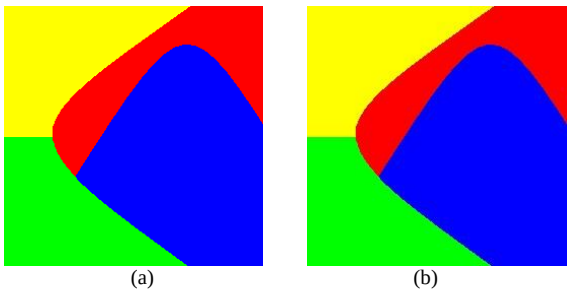

(a) (b)

Fig. 17. Ground truth of Simulated SAR images 1-SI1. (a) Ground truth; (b) Ground truth with speckle noise.

The test results of the proposed method and the compared algorithms on the ground truth with speckle noise are listed in table VII.

TABLE VII RESULTS OF 1-SI1 ON THE GROUND TRUTH WITH SPECKLE NOISE

Algorithms	CKSFCM	NSFCM	ALFCM	FKPFCM	PHFCM	THFCM
SA(%)	69.81	62.57	72.93	70.47	73.06	**75.77**

The segmentation results of the algorithms on ground truth with speckle noise in Table VII is lower than those shown in Table II. The proposed THFCM and the compared NSFCM, FKPFCM and PHFCM are around 3% lower than what there are on the ground truth without speckle noise. The larger reduction arose on the algorithms with homogeneous segmentation result, such as THFCM and PHFCM. The segmentation result with many coarse region is less affected by the speckle noise, such as CKSFCM and ALFCM. The segmentation accuracy of these two algorithms are around 1.5% lower than the result show in Table II. But the best segmentation accuracy among these methods is obtained by the proposed algorithm THFCM. This result indicates the robustness of the proposed algorithm.

J. Simulation results on single look dataset

In this section, we perform the critical case experiment on single look dataset to show the performance of the proposed THFCM on challenge situation. The single look dataset is employed in this paper shown in Fig. 18. There are four different regions, which are respectively marked by four different colors named red, blue, green and yellow in the result map of the proposed and compared algorithms. The size of this image is 512 * 512 and the resolution is 0.5 meter. As the single look dataset, there are also many irregular regions compared with the former real SAT images. Thus, this dataset can reflect the performance of algorithms more objectively.

Fig. 18 Sing look SAR image.

The parameters of THFCM P, B and L are set as 3, 5 and 3 respectively. The segmentation result of the proposed THFCM under the choice of parameters and the compared algorithms while the parameters set same as they are in the corresponding reference shown in Fig. 19.

It can be seen from Fig. 19 that each algorithm has the miss-segmentation regions, which mainly appear in the brighter regions in Fig. 18 for the speckle noise. Compared with other algorithms, PHFCM performs the more accurate segmentation result map. But many information on the boundary is missed for it uses regular square pixel patches for clustering. For NSFCM and ALFCM, a large number pixels are miss-segmentation among each class region. This phenomenon, however, can be found more usual in Fig. 19 (f) for there are many speckle noise compared with multi look datasets. As for the proposed THFCM, the results show that the algorithm is better than the compared algorithms in the discrimination between classes and homogenization in each class.

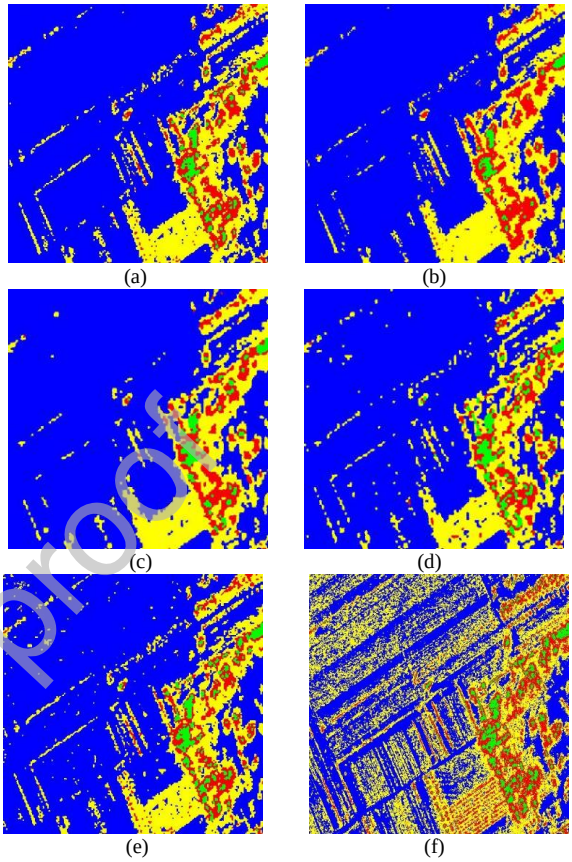

Fig. 19. Segmentation result maps of the six algorithms on single look dataset. (a) THFCM; (b) PHFCM; (c) FKPFCM; (d) NSFCM; (e) ALFCM; (f) CKSFCM.

IV. CONCLUSION

In this paper, an unsupervised thumbnail-based hierarchical fuzzy clustering method THFCM has been proposed for SAR image segmentation. The method constructs thumbnails for the input SAR image by using the major pixels in pixel groups, and using the thumbnails' clustering results to hierarchically segment the input SAR image. The process of generating and clustering thumbnails is capable of incorporating a combination of both local and non-local information in the image. This combination of data reduces the adverse influence of speckle noise on the segmentation result. It also reduces the computational time spent on the clustering operation and greatly improves the segmentation efficiency. We have performed experiments on three simulated SAR images, with different numbers of looks, and four real SAR images, comparing the performance of THFCM against five state-of-the-art algorithms. The experiments show that our proposed method has observable superiority in terms of running time and segmentation accuracy.

In future work, the ideas of this paper can be combined with other algorithms and used in other images. Some possible

extensions include the following. 1) By extracting effective semantic features using a variety of possible methods, each pixel could be represented by a feature vector. An interesting extension of this work, would be to segment the image using the method proposed in this paper, while changing the clustering element into a vector, rather than a scalar pixel intensity value. 2) By judging the complexity of the region to which every pixel belongs, the image can be divided into homogeneous and non-homogeneous regions in advance. Then we can segment these different regions separately. At this time, the ideas of the pixel groups and thumbnails can also be used to improve the segmentation efficiency.

Declaration of interests

☑The authors declare that they have no known competing financial interests or personal relationships that could have appeared to influence the work reported in this paper.

A. CRediT Author Statement

Ronghua Shang:Conceptualization, Software, Resources, Writing - Review & Editing, Project administration. **Guangguang Wang**: Methodology, Formal analysis, Investigation, Writing - Review & Editing, Visualization. **Chen Cheng**: Methodology, Validation, Formal analysis, Writing - Original Draft. **Kaiming Xu**: Validation, Investigation, Data Curation. **Licheng Jiao**: Resources, Supervision, Project administration, Funding acquisition. **Michael Aggrey Okoth:** Writing- Review & Editing. **Rustam Stolkin**: Writing - Review & Editing

ACKNOWLEDGEMENT

We would like to express our sincere appreciation to the editors and the anonymous reviewers for their insightful comments, which have greatly helped us in improving the quality of the paper. This work was partially supported by the National Natural Science Foundation of China under Grants Nos. 61773304, 61836009, 61871306, 61772399 and U1701267, the Fund for Foreign Scholars in University Research and Teaching Programs (the 111 Project) under Grants No. B07048, and the Program for Cheung Kong Scholars and Innovative Research Team in University under Grant IRT1170.

REFERENCES

[1] A. Raeisi, G. Akbarizadeh, and A. Mahmoudi, "Combined method of an efficient Cuckoo search algorithm and nonnegative matrix factorization of different Zernike moment features for discrimination between oil spills and lookalikes in SAR images", *IEEE J. Sel. Topics Appl. Earth Observ. Remote Sens.*, vol. 11, no. 11, pp. 1-13, July. 2018.

[2] Y. Yang, X. Cong and K. Long, "MRF model-based joint interrupted SAR imaging and coherent change detection via variational Bayesian inference," *Signal Process.*, pp. 144-154, 2018.

[3] J. Han, D. Zhang, G. Cheng, L. Guo and J. Ren, "Object Detection in Optical Remote Sensing Images Based on Weakly Supervised Learning and High-Level Feature Learning," *IEEE Trans. Geosci. Remote Sensing*, vol. 53, no. 6, pp. 3325-3337, Jun. 2015.

[4] L. Wan, T. Zhang and Y. Xiang "A robust fuzzy C-means algorithm based on bayesian non-local spatial information for SAR image segmentation," *IEEE J. Sel. Topics Appl. Earth Observ. Remote Sens.*, vol. 3, no. 4, pp. 896-906, Mar. 2018.

[5] Y. Zheng, X. Wang, G. Zhang, B. Xiao and F. Xiao. "Multi-Kernel Coupled Projections for Domain Adaptive Dictionary Learning," *IEEE Trans. Multimedia*, vol. 21, no. 9, pp. 2292-2304, Sep. 2019.

[6] R. H. Nobre, F. A. A. Rodrigues, R. C. P. Marques, J. S. Nobre, J. F. S. Rocha Neto, and F. N. Medeiros, "SAR image segmentation with Rényi's entropy," *IEEE Signal Process Lett*, vol. 23, no. 11, pp. 1551-1555, Nov. 2016.

[7] Q. Gao, Y. Lu and D. Sun, "Directionlet-based denoising of SAR images using a Cauchy model," *Signal Process.*, vol. 93, no. 5, pp. 1056-1063, 2013.

[8] F. A. A. Rodrigues, J. F. S. R. Neto, R. C. P. Marques, F. N. S. de Medeiros, and J. S. Nobre, " SAR image segmentation using the roughness information," *IEEE Geosci. Remote Sens. Lett.*, vol. 13, no. 2, pp. 132-136, Feb. 2016.

[9] Y. Zheng, L. Sun, S. Wang and J. Zhang. "Spatially Regularized Structural Support Vector Machine for Robust Visual Tracking," *IEEE Trans. Neural Netw. Learn. Syst.* Vol. 30, no. 10, Oct, 2019.

[10] G. Akbarizadeh, "A new statistical-based Kurtosis wavelet energy feature for texture recognition of SAR images," *IEEE Trans. Geosci. Remote Sens.*, vol. 50, no.11, 4358-4368, 2012.

[11] Z. Tirandaz and G.Akbarizadeh, "A two-phase algorithm based on kurtosis curvelet energy and unsupervised spectral regression for segmentation of SAR images. *IEEE J. Sel. Topics Appl. Earth Observ. Remote Sens.*, vol. 9, no.3, pp.1244-1264, 2016.

[12] Z. Tirandaz and G. Akbarizadeh, "Unsupervised texture-based SAR image segmentation using spectral regression and Gabor filter bank," *J. Indian Soc. Remote Sens.*, vol. 44, no. 2, pp. 177-186, 2016.

[13] Y. Gui, X. Zhang, Y. Shang, et al. "SAR image segmentation using MSER and improved spectral clustering," *EURASIP J. Adv. Signal Process.*, vol. 2011, no. 1, pp.83-101, Jan. 2012.

[14] G. R. K. S. Subrahmanyam, A. N. Rajagopalan, and R. Aravind, "A recursive filter for despeckling SAR images," *IEEE T. Image Process.*, vol. 17, no. 10, pp. 1969-1974, Oct. 2008.

[15] H. Li, H. Qiu and Z. Yu, "Multifocus image fusion via fixed window technique of multiscale images and non-local means filtering," *Signal Process.*, pp. 71-85, 2017,

[16] J. Gu, L. Jiao, S. Yang,F. Liu, B. Hou, and Z. Zhao, "A multi-kernel joint sparse graph for SAR image segmentation," *IEEE J. Sel. Topics Appl. Earth Observ. Remote Sens.*, vol. 9, no. 3, pp. 1265-1285, Mar. 2016.

[17] A. Dempster, "Maximum likelihood from incomplete data via the EM algorithm," *J. Roy. Statist. Soc.*, vol. 39, no. 1, pp. 1-38, 1977.

[18] J. Kitler, and J. Ilingworth, "Minimum error thresholding,"

Pattern Recognit., vol. 19, no. 1, pp.41-47, 1986.

[19] M. Kass, A. Witkin, D. Terzopoulos. "Snakes: Active contour models," *Int. J. Comput. Vis.*, vol. 1, no. 4, pp.321-331, 1988.

[20] R. C. P. Marques, F. N. S. Medeiros, and J. S. Nobre, "SAR image segmentation based on level set approach and G0A mode," IEEE Trans. Pattern Anal. Mach. Intell., vol. 34, no. 0, pp. 2046-2057, Oct. 2012.

[21] H. Song, B. Huang, and K. Zhang, "A globally statistical active contour model for segmentation of oil slick in SAR imagery," *IEEE J. Sel. Topics Appl. Earth Observ. Remote Sens.*, vol. 6, no. 6, pp. 2402-2409, Apr. 2013.

[22] L. A. Vese and T. F. Chan, "A multiphase level set framework for image segmentation using the Mumford and Shah model," *Int. J. Comput. Vis.*, vol. 50, no. 3, pp. 271-293, 2002.

[23] J. F. S. R. Neto, A. M. Braga, F. N. S. de Medeiros, and R. C. P. Marques, "Level-set formulation based on Otsu method with morphological regularization," in Proc. *IEEE Int. Conf. Image Process.* (ICIP), Sep. 2017, pp. 2144-2148.

[24] F. Wang, Y. Wu, M. Li, P. Zhang, and Q. Zhang, "Adaptive hybrid conditional random field model for SAR images Segmentation," *IEEE T. Geosci. Remote Sens.*, vol. 55, no. 1, pp. 537-550, Jan. 2017.

[25] P. Zhan, M. Li, Y. Wu, L. Gan, and M. Liu, "Unsupervised multi-class segmentation of SAR images using fuzzy triplet Markov fields model," *Pattern Recognit.*, vol. 45, no. 11, pp. 4018-4033, 2012.

[26] P. Zhang, M. Li, Y. Wu, and H. Li, "Hierarchical conditional random fields model for semi supervised SAR image segmentation," *IEEE T. Geosci. Remote Sens.*, vol. 53, no. 9, pp. 4933-4951, Sept. 2015.

[27] S. Gou, X. Zhuang, H. Zhu, and T. Yu, "Parallel sparse spectral clustering for SAR image segmentation," *IEEE J. Sel. Topics Appl. Earth Observat. Remote Sens.*, vol. 6, no. 4, pp. 1949-1963, Aug. 2013.

[28] Y. Zhong, A. Ma, and L. Zhang, "An adaptive memetic fuzzy clustering algorithm with spatial information for Remote Sensing Imagery," *IEEE J. Sel. Topics Appl. Earth Observ. Remote Sens.*, vol. 7, no. 4, pp. 1235-1248, Apr. 2014.

[29] D. L. Pham. "Spatial models for fuzzy clustering," *Comput. Vis. Image Und.*, vol. 84, no. 2, pp. 285-297, 2001.

[30] J. Feng, L. Jiao, and X. Zhang, "Robust non-local fuzzy c-means algorithm with edge preservation for SAR image segmentation," *Signal Process.*, vol. 93, no. 2, pp. 487-499, 2013.

[31] Z. Gao, W. Hua, M. Lu and Y. Zhang, "automated framework for detecting lumen and media-adventitia borders in intravascular ultrasound images," *Ultrasound in Medicine & Biology*, vol. 41, no. 7, pp. 2001-2021, Jul. 2015.

[32] D. Xiang, T. Tang, C. Hu, Y. Li, and Y. Su, "A kernel clustering algorithm with fuzzy factor: application to SAR image segmentation," *IEEE Geosci. Remote Sens. Lett.*, vol. 11, no. 7, pp. 1290-1294, Jul. 2014.

[33] W. Cai, S. Chen, and D. Zhang, "Fast and robust fuzzy c-means clustering algorithms incorporating local information for image segmentation," *Pattern Recognit.*, vol. 40, no. 3, pp. 825-838, Mar. 2007.

[34] S. Krinidis and V. Chatzis, "A robust fuzzy local information C-means clustering algorithm," *IEEE T. Image Process.*, vol. 19, no. 5, pp. 1328-1337, Jan. 2010.

[35] H. Zhang, Q. Wang and W. Shi, "A novel adaptive fuzzy local information C -means clustering algorithm for remotely sensed imagery classification," *IEEE Trans. Geosci. Remote Sensing*, vol. 55, no. 9, pp. 5057-5068, Sept. 2017.

[36] M. Gong, L. Su, M. Jia, and W. Chen, "Fuzzy clustering with a modified MRF energy function for change detection in synthetic aperture radar Images," *IEEE T. Fuzzy Sys.*, vol. 22, no. 1, pp. 98-109, Feb. 2013.

[37] X. Zhang, H. Li, and C. Qi, "Spatially constrained fuzzy clustering based sensor placement for spatiotemporal fuzzy-control system," *IEEE T. Fuzzy Sys.*, vol. 18, no. 5, pp. 946-957, Oct. 2010.

[38] Z. Ju and H. Liu, "A unified fuzzy framework for human-hand motion recognition," *IEEE T. Fuzzy Sys.*, vol. 19, no. 5, pp. 901-913, Oct. 2011.

[39] R. Shang, P. Tian, L. Jiao, R. Stolkin, J. Feng, B. Hou, and X. Zhang, "A spatial fuzzy clustering algorithm with kernel metric based on immune clone for SAR image segmentation," *IEEE J. Sel. Topics Appl. Earth Observ. Remote Sens.*, vol. 9, no. 4, pp. 1640-1652, Apr. 2016.

[40] J. Ji and K. Wang, "A robust non-local fuzzy clustering algorithm with between-cluster separation measure for SAR image segmentation," *IEEE J. Sel. Topics Appl. Earth Observ. Remote Sens.*, vol. 7, no. 12, pp. 4929-4936, Dec. 2014.

[41] G. Liu, Y. Zhang, and A. Wang, "Incorporating adaptive local information into fuzzy clustering for image segmentation," *IEEE T. Image Process.*, vol. 24, no. 11, pp. 3990-4000, Nov. 2015

[42] R. Shang, Y. Yuan, L. Jiao, B. Hou, A. M. G. Esfahani, and R. Stolkin, "A fast algorithm for SAR image segmentation based on key pixels," *IEEE J. Sel. Topics Appl. Earth Observ. Remote Sens.*, vol. 10, no. 12, pp. 5657-5673, Oct. 2017.

[43] C. A. Deledalle, L. Denis, G. P. F.Tupin, and L. Verdoliva, "Exploiting patch similarity for SAR image processing: the non-local paradigm," *IEEE Signal Proc. Mag.*, vol. 31, no. 4, pp. 69-78, Jun. 2014.

[44] J. Geng, H. Wang, J. Fan, and X. Ma, "Deep supervised and contractive neural network for SAR image classification," *IEEE T. Geosci. Remote Sens.*, vol. 55, no. 4, pp. 2442-2459, Jan. 2017.

[45] S. Dong, Z. Gao, S. P and W. Wu, "IoT-based 3D convolution for video salient object detection," Neural Comput. Appl, Jan. 2019.

[46] W. Wang, D. Xiang and Y. Ban, "Superpixel Segmentation of Polarimetric SAR Images Based on Integrated Distance Measure and Entropy Rate Method," *IEEE J. Sel. Topics Appl. Earth Observ. Remote Sens.*, vol. 10, no. 9, pp. 4045 - 4058, Jun. 2017.

[47] D. Xiang, T. Tang, S. Quan, D. Guan and Y. Su, "Adaptive Superpixel Generation for SAR Images with Linear Feature Clustering and Edge Constraint," *IEEE Trans. Geosci. Remote Sensing*, vol. 57, no. 6, June. 2019.

[48] R. Achanta, A. Shaji, K. Smith, A. Lucchi, and P. Fua, "Slic superpixels compared to state-of-the-art superpixel methods," *IEEE Trans. Pattern Anal. Mach. Intell.*, vol. 34, no. 11, pp. 2274-82,2012.

[49] Y. Guo, L. Jiao, and S. Wang. "Fuzzy-Superpixels for Polarimetric SAR Images Classification," *IEEE T. Fuzzy Sys.*, PP.99:1-1, 2018.

[50] J. Han, K. N. N, M. Li and H. Zhang, "Unsupervised Extraction of Visual Attention Objects in Color Images," *IEEE Trans. Circuits Syst. Video Technol.* vol. 16, no. 1, Jan. 2006.

[51] J. Geng, X. Ma, J. Fan, and H. Wang, "Semisupervised classification of polarimetric SAR image via superpixel restrained deep neural network," *IEEE Geosci. Remote Sens. Lett.*, vol. 15, no. 1, pp. 122-126, Jan. 2018.

[52] G. Gao, "Statistical modeling of SAR images: A survey," *Sensors*, vol. 10, no. 1, pp. 775-795, Jan. 2010.

[53] Y. Yu and S. T. Acton, "Speckle Reducing Anisotropic Diffusion," *IEEE T. Image Process.*, vol. 11, no. 11, pp. 1260-1270, Nov. 2002.

[54] A. Frery, H.-J. Müller, C. C. F. Yanasse, and S. J. S. Sant'Anna, "A model for extremely heterogeneous clutter," *IEEE Trans. Geosci. Remote Sens.*, vol. 35, no. 3, pp. 648-659, May 1997.

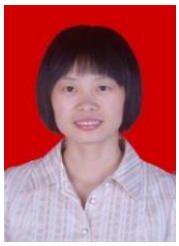

Ronghua Shang (M'09) received the B.S. degree in information and computation science and the Ph.D. degree in pattern recognition and intelligent systems from Xidian University in 2003 and 2008, separately.
She is currently a professor of Xidian University. Her current research interests include, evolutionary computation, image processing, and data mining.

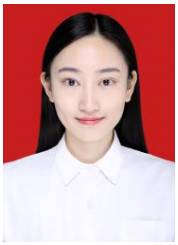

Chen Chen received the B.E. degree in School of Intelligent Science and Technology from Xidian University, Xi'an, China. Now she is pursuing the M.S. degree in school of Electronic Communication Engineering from Xidian University, Xi'an, China. Her current research interests include image processing and machine learning.

Guangguang Wang received the B.E. degree in electronic information science and technology from the School of Information Engineering, Inner Mongolia University Of Technology, Hohhot, China in 2017.
He is currently working toward the M.S. degree in electronic circuit and system at the School of Artificial intelligence, Xidian University, Xi'an, China.

Licheng Jiao (SM'89) received the B.S. degree from Shanghai Jiaotong University, Shanghai, China, in 1982, the M.S. and Ph.D. degrees from Xi'an Jiaotong University, Xi'an, China, in 1984 and 1990, separately. From 1990 to 1991, he was a postdoctoral Fellow in the National Key Laboratory for Radar Signal Processing, Xidian University, Xi'an, China. Since 1992, Dr. Jiao has been a Professor in the School of Electronic Engineering at Xidian University. Currently, he is the Director of the Key Lab of Intelligent Perception and Image Understanding of Ministry of Education of China at Xidian University, Xi'an, China. Dr. Jiao is a Senior Member of IEEE, member of IEEE Xi'an Section Execution Committee and the Chairman of Awards and Recognition Committee, vice board chairperson of Chinese Association of Artificial Intelligence, councilor of Chinese Institute of Electronics, committee member of Chinese Committee of Neural Networks, and expert of Academic Degrees Committee of the State Council.

His research interests include image processing, natural computation, machine learning, and intelligent information processing. He has charged of about 40 important scientific research projects, and published more than 20 monographs and a hundred papers in international journals and conferences.

Michael Aggrey Okoth received the B.E. degree in Electronic&Information Engineering from Xidian University Xi'an China in 2015 and the M.E degree in Electronic Science and Technology from Xidian University Xi'an China in 2018.

He is currently pursuing Ph.D. degree in School of Artificial Intelligence from Xidian University, Xi'an China and his research interest is Evolutionary Computation.

Rustam Stolkin (M'12) received an MEng degree in engineering science from the University of Oxford, U.K., in 1998, and a Ph.D. in computer vision from University College London, U.K., in 2004.

He is currently Director of UK's National Centre for Nuclear Robotics, Royal Society Industry Fellow, and Professor of Robotics at University of Birmingham, where he is founder and director of the Extreme Robotics Lab (ERL). He is also Director of spinout company A.R.M Robotics Ltd.